

HIGH-RATE LOCAL SEA LEVEL MONITORING WITH A GNSS-BASED TIDE GAUGE

Johan S. Löfgren, Rüdiger Haas, Jan M. Johansson

Chalmers University of Technology
Department of Earth and Space Sciences
Onsala Space Observatory, SE-439 92 Onsala, Sweden

ABSTRACT

We present first results from the analysis of high-rate observations with a GNSS-based tide gauge at the Onsala Space Observatory. The goal is to determine local sea level with high temporal resolution. The GNSS-based tide gauge makes use of right-hand circular polarized GNSS signals that are directly received and left-hand circular polarized GNSS signals that are reflected from the sea surface. An experimental setup of the GNSS-based tide gauge was operated in the spring of 2010 and data were recorded with a sampling rate of 20 Hz. We analyzed data decimated to 1 Hz using different temporal resolution between 5 and 240 seconds, and the resulting time series of local sea level were compared to each other and to results from two stilling well gauges. The comparison with the data from the stilling well gauges shows a common trend. The comparison of the results from analyses with different temporal resolution show consistent results. There is also an indication that the GNSS-based tide gauge might be able to give information on the sea surface state.

Index Terms— GNSS, reflected signals, local sea level, tide gauge

1. INTRODUCTION

It is important for human society to continuously monitor the sea level, since it is an indicator of global climate change. There are several effects of global warming that will impact the sea level [1], e.g., the melting of large masses of ice in polar and subpolar regions which brings freshwater into the ocean, thermal expansion of sea water, and changes in atmospheric and ocean circulation. Furthermore, changes in the sea level has important consequences for human society, e.g., [10] predicted that up to 332 million people in coastal and low-lying areas will be directly affected by flooding from sea level rise by the end of the 21st century. Additionally, the displacement of these people will affect millions more.

Tide gauges are traditionally used to monitor local sea level by measuring the vertical distance between the sea surface and the land surface. This observation, directly related to the volume of the ocean, results in values relative to the Earth's crust, which is itself in motion on longer

timescales [9, 4]. Therefore, in order to fully understand the underlying processes, it is useful to separate the observation into local land surface height and local sea surface height. This can be done with satellite techniques, e.g., Global Navigation Satellite Systems (GNSS), observing both the directly received GNSS signals, to obtain land surface heights, and reflected GNSS signals from the sea surface, to obtain sea surface heights, and relating them to the Earth's center of mass. Combining both measurements will then result in measurements of local sea level.

This type of GNSS-based tide gauge was proposed by [5, 6] and it was shown to have a RMS-differences of less than 4 cm compared to hourly values from two stilling well gauges located 18 km and 33 km away from the tide gauge site.

Here we present first results of high-rate sea level measurements with a similar measurement setup, and compare these to observations from the same two stilling well gauges. We analyze measurements with different temporal resolution.

2. CONCEPT

The GNSS-based tide gauge as presented by [5, 6] consists of two antennas mounted back-to-back on a beam over the ocean (see Fig. 1). The zenith-looking antenna is right hand circular polarized (RHCP), receiving the direct GNSS-signals, whereas the nadir-looking antenna is left hand circular polarized (LHCP), receiving the signals that are reflected from the sea surface. The antennas are mounted so that the phase centers are aligned along the local vertical. Thus, they differ only in vertical position, since there is no horizontal difference between the antennas. Each antenna is connected to a standard geodetic-type two-frequency GNSS receiver.

Since the reflected signals experience an additional path delay ($a + b = c$) compared to the directly received signals, the LHCP antenna can also be regarded as a virtual antenna located below the sea surface (see Fig. 1). The height of the LHCP antenna over the sea surface (h) can be expressed as

$$h = \frac{a + b}{2 \sin \varepsilon} - \frac{d}{2} \quad (1)$$

where ε is the elevation of the transmitting satellite, $a + b = c$ is the additional path delay of the reflected signal, and d is the

vertical separation between the phase centers of the RHCP and the LHCP antennas. When the sea level changes, the path delay of the reflected signal changes and thus, the LHCP antenna will appear to change vertical position. The vertical difference in position between the RHCP and the LHCP antenna (Δv) can then be expressed as $\Delta v = 2h + d$ and as a result, the installation monitors changes in local sea level.

In Fig. 1 it is assumed that the sea surface is flat compared to the signal wavelength. This means that the signal energy is reflected coherently towards the antenna. However, the distribution of the reflected energy is governed by the surface roughness, the signal wavelength, and the elevation angle, e.g., for a fixed elevation angle, a high surface roughness will spread the reflected signal more in space than a low surface roughness (see e.g. [8]). This will give the effect that for large sea surface roughnesses, the received signal energy is low and therefore the receivers will have difficulties to keep continuous lock to the satellite signals.

Multiple satellites with different elevation and azimuth angles are observed each epoch and this means that the estimated change in sea level can not be considered to originate from one specific point on the sea surface. Instead it represents the change of an average sea surface plane formed by the reflection points, where the distribution of these points is limited by the placement of the antenna and the antenna geometry. For a fixed antenna height, the average plane will change during different stages of the site's tidal cycle.

3. EXPERIMENTAL SETUP

A setup of the GNSS-based tide gauge was installed in February 2010 at the Onsala Space Observatory (OSO) at the Swedish west coast. The antenna installation was mounted with open sea in the southward direction and the downward-looking LHCP antenna was positioned approximately 1 m over the sea surface (at the time of installation). Both antennas were protected by hemispherical radomes, see Fig. 2.

Data were collected during approximately 4 months using one Leica GRX1200+ receiver connected to the RHCP antenna (Leica AR25 multi-GNSS choke-ring) and one Leica GRX1200 receiver connected to the LHCP antenna (Leica AR25 multi-GNSS choke-ring). Both receivers recorded data with 20 Hz sampling. During the first 6 weeks of the experiment the coastal waters were frozen, and the sea ice did not melt completely before the middle of March.

4. DATA ANALYSIS

The data were first decimated into 1 Hz data, for faster processing, using the Translation, Editing, and Quality Check (TEQC) software [3]. Thereafter an elevation and azimuth mask was applied to the data, removing data below 20° elevation and outside the southeast direction -135° to

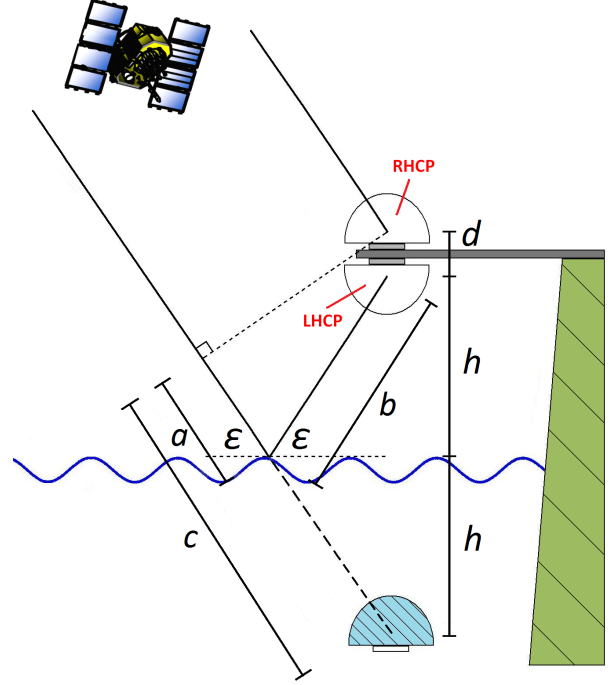


Fig. 1. Schematic drawing of the GNSS-based tide gauge. The installation consists of two antennas (one RHCP and one LHCP), mounted on a beam over the ocean at the height h over the sea surface. The LHCP antenna receives the signals reflected from the sea surface whereas the RHCP antenna receives the direct signals.

$+45^\circ$ azimuth. This was done to remove unwanted signals according to [5].

An in-house developed software in MATLAB was used to analyse the data with relative positioning using least squares solutions. The software used GPS L1 phase delay single differences together with IGS satellite ephemerides [2] according to

$$\lambda \Phi_{AB}^j(t) = \varrho_{AB}^j(t) + \lambda N_{AB}^j + c \delta_{AB}(t) \quad (2)$$

where λ is the wavelength of the L1 carrier, $\Phi_{AB}^j(t)$ is the difference in the measured carrier phase expressed in cycles, $\varrho_{AB}^j(t)$ is the difference in geometry in meters, N_{AB}^j is the difference in phase ambiguity in cycles, c is the speed of light in vacuum, and $\delta_{AB}(t)$ is the difference in receiver clock bias. A and B denotes the two receivers and j denotes the satellite used in the single difference. Because of the very short baseline between the receivers, both tropospheric and ionospheric effects can be ignored in Eq. 2.

The difference in geometry can then be expressed in a local coordinate system using azimuth α and elevation ε for each satellite as

$$\varrho_{AB}^j(t) = -\Delta e \sin \alpha^j \cos \varepsilon^j - \Delta n \cos \alpha^j \cos \varepsilon^j - \Delta v \sin \varepsilon^j \quad (3)$$



Fig. 2. The experimental setup of the GNSS-based tide gauge at the Onsala Space Observatory with the radome of the 20 m geodesy/astronomy radiotelescope in the background towards the east. There is open sea towards the south.

where Δe , Δn , and Δv are the east, north, and vertical components of the baseline between the two receivers. Because of the vertical alignment of the antennas, the horizontal baseline components are zero and can be removed from Eq. 3.

The processing was carried out in two steps. Firstly, a least squares approach was used to solve Eq. 2 for float ambiguity differences for each satellite pair, the mean vertical baseline component for all epochs, and receiver clock differences for each epoch. Secondly, the determined float ambiguities were inserted as known parameters into Eq. 2 and thus removed from the following calculations. The remaining linear system of equations was then solved again with a least squares approach, this time estimating only for receiver clock differences for each epoch and vertical baseline components for a desired number of epochs. This means that we were able to produce several solutions with different temporal resolution for the vertical baseline component. We performed solutions with a temporal resolution of 5, 30, 60, 120, and 240 seconds and converted these into time series of local sea level h (see Section 2).

Since there were no ice level data to compare with the results from the GNSS-based tide gauge (the Swedish Meteorological and Hydrological Institute (SMHI) only provides sea level) we concentrated on open water conditions and did not analyze data observed under sea ice conditions.

5. RESULTS

Figure 3 shows about 40 minutes of GNSS-derived local sea level with temporal resolution between 5 and 240 seconds together with independent sea level data from two stilling well gauges. The two stilling well gauges have a temporal resolution of 600 seconds and are operated by SMHI at Ringhals and Göteborg, about 18 km south of and 33 km north of OSO, respectively. Since the GNSS-based tide gauge observations are relative to the position of the RHCP antenna and the SMHI measurements refer to the mean sea level of the year, mean values were removed from each time series.

Comparing the GNSS-derived time series with the stilling well gauge data it is apparent that there is some agreement between the time series. An overall negative trend can be seen, which could correspond to a more large scale water movement. However, the GNSS-based time series appear to have a larger range and since the temporal resolution is higher, more fine scale variations are seen. Since OSO, Ringhals and Göteborg are separated by several km, also hydrodynamic differences can be expected.

In order to compare the time series of the different temporal resolutions, the 30, 60, 120, and 240 second series were linearly interpolated to the same resolution as the time series with 5 seconds temporal resolution and pairwise root-mean-square (RMS) differences were calculated, see Tab. 1. The RMS-differences between the time series with 5 seconds tem-

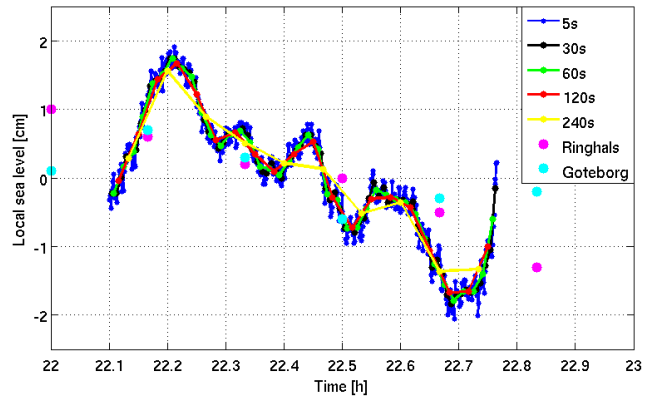


Fig. 3. Time series of local sea level with the temporal resolution of 5, 30, 60, 120, and 240 seconds together with sea level measurements from stilling well gauges (18 km and 22 km from OSO) with the temporal resolution of 600 seconds. The mean is removed from each time series.

Table 1. Pairwise RMS differences between the different temporal resolutions. Values are in millimeters.

		temporal resolution (s)			
		30	60	120	240
temporal resolution (s)	5	1.3	1.4	1.7	2.8

poral resolution and those with 30, 60 and 120 seconds temporal resolution are approximately on the same order of magnitude. However, the RMS-difference increases by about 50% when comparing the time series with temporal resolutions of 5 seconds and 240 seconds. This could be an indication for the detection of waves with periods longer than 120 seconds and mean that the results from the GNSS-based tide gauge can be used to characterize the sea surface state.

6. CONCLUSIONS AND OUTLOOK

The presented results show that it is possible to observe and analyze high-rate data from the GNSS-based tide gauge and to derive local sea level with different temporal resolution. The results from analyses with different temporal resolution are consistent. Furthermore, there is some indication that results with different temporal resolution can be used to characterize the sea surface state.

The comparison of the GNSS-based times series of local sea level with independent data from two stilling well gauges of lower temporal resolution shows a similar trend. However, the local short-time sea level variations at the Onsala Space Observatory can not be represented by observations with low temporal resolution 18 km to 33 km away.

For the future, we will continue to analyze the high-rate GNSS data with sampling rates of up to 20 Hz. We plan to analyze long time series and use different temporal resolution. In order to increase the number of reflection points each epoch it would be beneficial to incorporate data from other GNSS like Glonass (and in the future Galileo) into the analysis.

For comparison purposes, we will install a pressure-based tide gauge at OSO, co-located with the GNSS-based tide gauge. This will allow a more accurate assessment of the method in the same coastal area and with the same temporal resolution.

7. REFERENCES

- [1] N.L. Bindoff, J. Willebrand, V. Artale, A. Cazenave, J. Gregory, S. Gulev, K. Hanawa, C. Le QuZrZ, S. Levitus, Y. Nojiri, C.K. Shum, L.D. Talley and A. Unnikrishnan, "Observations: Oceanic climate change and sea level", in *Climate Change 2007: The Physical Science Basis*, Contribution of Working Group I to the Fourth Assessment Report of the Intergovernmental Panel on Climate Change, edited by S. Solomon, D. Qin, M. Manning, Z. Chen, M. Marquis, K. B. Averyt, M. Tignor, and H. L. Miller, Cambridge University Press, Cambridge, United Kingdom and New York, NY, USA, 2007.
- [2] J.M. Dow, R.E. Neilan, and C. Rizos, "The International GNSS Service in a changing landscape of Global Navigation Satellite Systems", *J. Geod.*, vol. 83, pp. 191–198, 2009.
- [3] L.H. Estey, and C.M. Meertens, "TEQC: The multi-purpose toolkit for GPS/GLONASS data", *GPS Solutions*, vol. 3(1), pp. 42–49, 1999.
- [4] J.M. Johansson, J.L. Davis, H.-G. Scherneck, M. Vermeer, J. Mitrovica, R. Bennet, B. Jonsson, G. Elgered, P. Elosegui, H. Koivula, M. Poutanen, B. Rönnäng and I. I. Shapiro, "Continuous GPS measurements of postglacial adjustment in Fennoscandia, 1. Geodetic results", *J. Geophys. Res. (Solid Earth)*, vol. 107, 2157, 2002.
- [5] J.S. Löfgren, R. Haas, and J.M. Johansson, "Sea Level Monitoring Using a GNSS-Based Tide Gauge", in *Proceedings of 2nd International Colloquium - Scientific and Fundamental Aspects of the Galileo Programme*, Proceedings CD-ROM, European Space Agency, 2009.
- [6] J.S. Löfgren, R. Haas, and J.M. Johansson, "Monitoring Coastal Sea Level Using Reflected GNSS Signals", submitted to *Advances in Space Research*, 2010.
- [7] M. Martin-Neira, P. Colmenarejo, G. Ruffini G., C. Cerra, "Altimetry precision of 1 cm over a pond using the wide-lane carrier phase of GPS reflected signals", *Can. J. Remote Sens.*, vol. 28(3), pp. 394–403, 2002.
- [8] W.G. Rees, "Physical principles of remote sensing", second edition, University press, Cambridge, United Kingdom, 2003.
- [9] H.-G. Scherneck, J.M. Johansson, G. Elgered, J.L. Davis, B. Jonsson, G. Hedling, H. Koivula, M. Ollikainen, M. Poutanen, M. Vermeer, J.X. Mitrovica, and G.A. Milne, "BIFROST: Observing the three-dimensional deformation of Fennoscandia", in *Ice Sheets, Sea Level and the Dynamic Earth*, J. X. Mitrovica and B. Vermeersen (Eds), AGU Geodyn. Ser. 29, 69–93. American Geophysical Union, Washington D.C., 2002.
- [10] K. Watkins, C. Ugaz, L. Carvajal, D. Coppard, R.F. Nieva, A. Gaye, W. Ha, C. Johansson, A. Kennedy, C. Kuonqui, I.M. Pereira, R. Menon, J. Morse, and P. Seck, "Human Development Report 2007/2008 - Fighting climate change: Human solidarity in a divided world", Palgrave Macmillan, New York, USA, for United Nations Development Programme, Available at <http://hdr.undp.org/en/reports/global/hdr2007-2008/>, 2007.